crystals

MDPI

Article

Development of Cerium Oxide/Chitosan/Graphene Oxide Nanocomposite: An Investigation toward Its Biological Applications under In Vitro Conditions

J. Saranya [1,*], S. Preethi [1], Mohammed Rafi Shaik [2,*], Merajuddin Khan [2], Mujeeb Khan [2] and Baji Shaik [3]

[1] Department of Electronics and Communication Engineering, Rajalakshmi Engineering College, Thandalam 602 105, Tamil Nadu, India; 210811001@rajalakshmi.edu.in
[2] Department of Chemistry, College of Science, King Saud University, P.O. Box 2455, Riyadh 11451, Saudi Arabia; mkhan3@ksu.edu.sa (M.K.); kmujeeb@ksu.edu.sa (M.K.)
[3] School of Chemical Engineering, Yeungnam University, Gyeongsan 38541, Republic of Korea; shaikbaji@yu.ac.kr
* Correspondence: saranya.j@rajalakshmi.edu.in (J.S.); mrshaik@ksu.edu.sa (M.R.S.)

Abstract: A ternary nanocomposite was prepared using cerium oxide, chitosan, and graphene oxide (CeO_2/CS/GO) using a simple and cost-effective wet chemical method. The physicochemical properties of the developed ternary nanocomposite were examined using X-ray diffraction, Fourier transform infrared spectroscopy, scanning electron microscopy with energy-dispersive X-ray spectroscopy, and ultraviolet-visible spectroscopy. Furthermore, the therapeutic behavior of the developed CeO_2/CS/GO composite was assessed using anti-bacterial, anti-fungal, and anti-cancer assays. For *Escherichia coli*, *Staphylococcus aureus*, and *Salmonella* species, 750 µg/mL of the CeO_2/CS/GO composite showed effective anti-bacterial activity, with a zone of inhibition of 9 mm. Additionally, the CeO_2/CS/GO composite's anti-fungal activity against *Aspergillus niger* was studied. The anti-cancer properties of different concentrations of the CeO_2/CS/GO composite were assessed on MCF-7 cells, and 18.8% of cells were found to be viable at the maximum concentration of 1000 µg/mL CeO_2/CS/GO and 46.37% at 125 µg/mL. The results of the hemolysis assay performed using human red blood cells and various concentrations of the CeO_2/CS/GO composite indicated that the nanocomposite possesses biological properties. Overall, it can act as a therapeutic platform for breast cancer, bacterial and fungal infections.

Keywords: MCF-7 cancer cells; CeO_2/CS/GO nanocomposite; anti-bacterial; anti-fungal; hemolysis; anti-cancer

Citation: Saranya, J.; Preethi, S.; Shaik, M.R.; Khan, M.; Khan, M.; Shaik, B. Development of Cerium Oxide/Chitosan/Graphene Oxide Nanocomposite: An Investigation toward Its Biological Applications under In Vitro Conditions. *Crystals* **2023**, *13*, 1393. https://doi.org/10.3390/cryst13091393

Academic Editor: Rajratan Basu

Received: 18 August 2023
Revised: 13 September 2023
Accepted: 15 September 2023
Published: 19 September 2023

1. Introduction

Nanotechnology is an interdisciplinary domain that focuses on providing solutions to diverse fields such as healthcare, pharmacy, biophysical modeling, biological engineering, and genetics [1]. The ability to apply surface-functionalized small-scale structures with novel features and the potential to control or manipulate organisms at the molecular or nanoscale level are the main areas of focus in contemporary nanotechnology. This will pave the way for the assessment of nanoplatforms as therapeutic agents [2]. Breast cancer is the most prevalent type of cancer and a major cause of mortality for women over 35 years of age. Nanotechnology enables therapeutic platforms on the nanoscale to selectively target and treat tumors. Validation of the developed nanoplatform as a therapeutic agent against breast cancer cell lines must be performed under both in vivo and in vitro conditions [3]. Several researchers have been interested in developing cerium oxide-based nanoplatforms (CeO_2 NPs) because of their distinct physicochemical properties, which play a vital role in their biological properties [4]. For example, the potential redox abilities of CeO_2 nanoparticles are responsible for their excellent antioxidant properties, which has been confirmed both

in vitro and in vivo [5]. In particular, CeO_2 exhibits interchangeable oxidation states of cerium (3+ and 4+ states) on the surface of the nanoparticle, wherein small CeO_2 NPs with larger surface areas possess a large number of 3+ sites [6]. These mixed valence states of Ce lead to the generation of oxygen vacancies and subsequently defects. In addition, owing to the adoption of fluorite crystal structures, CeO_2 NPs have been used in several fascinating fields, including biomedicine. However, the wider application of CeO_2 has been mainly inhibited by the aggregation of NPs, which is mainly addressed by modifying the surface of CeO_2 NPs using various materials, including carbonaceous substances and polymers, which effectively prevent aggregation and improve biocompatibility [7].

In this context, graphene has attracted significant attention owing to its excellent properties. Graphene is a two-dimensional sp^2-bonded carbon material with a honeycomb lattice structure. It is a fundamental component of graphitic substances and has attracted considerable interest owing to its unique properties. Graphene has a large surface-to-volume ratio, excellent tensile strength, chemical durability, and good thermal conductivity [8]. Graphene oxide (GO), an oxygenated derivative of graphene, harbors a large number of oxygen-containing groups on both the surface and edges of GO. These groups not only enhance the solubility and biocompatibility of materials but also collectively enhance the electronic and redox properties of the resulting composite materials [9]. According to Pang et al., the physicochemical characteristics of GO, such as size and length, surface characteristics, and aggregation factors, are primarily responsible for its anti-bacterial activity [10]. These factors affect the manner in which cells die after the deposition of bacteria onto the nanomaterials, which involves membrane breakdown once they touch the sharp edges of GO, leakage of cell contents into the environment, and ultimately cell death [11].

Moreover, CeO_2 has often been combined with other materials, particularly biomaterials, to fabricate multi-component composites with adequate sites for cell attachment and mechanical support [12]. For example, various biopolymers, including gelatin, collagen, alginate, and chitosan (CS), have been used to prepare CeO_2-based multicomponent composites with potential biological properties [13]. Chitosan is a linear polymer that resembles cellulose and has distinct chemical and biological properties as it contains amine and hydroxyl groups in its structure [14].

Owing to its outstanding biocompatibility, biodegradability, low toxicity, and inherent anti-bacterial activity, CS, a natural substance, has been extensively used in biomedical applications [15,16]. Due to their unique characteristics, such as high solubility and biocompatibility, antioxidant power, antimicrobial and anti-inflammatory properties, nanocomposites made from non-mineral nanoparticles loaded with natural biopolymers like chitosan are very effective for treating wound healing, cancer, inflammatory diseases, and cardiovascular conditions [17,18]. Furthermore, the anti-cancer activity of CS against hepatocellular carcinoma is mediated by a decrease in mitochondrial membrane potential, an increase in membrane lipid peroxidation, and neutralization of cell surface charge [19].

In a study, chitosan-coated cerium oxide (CS/CeO_2 NCs) derived from aqueous extracts of tea polyphenols were developed using a green synthesis route. With zones of inhibition of 13.5 ± 0.2 and 11.7 ± 0.2 mm, respectively, the developed CS/CeO_2 NCs showed outstanding antibacterial and antifungal activity against foodborne pathogens such as *Escherichia coli*, *Staphylococcus aureus*, and *Botrytis cinerea*. The findings showed that biosynthesized CS/CeO_2 NCs had the potential to be used as powerful antibacterial agents [20]. Chitosan-functionalized 2D layered MoS_2 hybrid nanocomposites were developed and subjected to in vitro assessment for their antibacterial and anticancer activities. The chitosan-MoS_2 hybrid nanocomposite exhibited zones of inhibition against *S. aureus* at 22, 28, and 32 mm and against *E. coli* at 26, 30, and 35 mm in the antibacterial application. The Chitosan-MoS_2 hybrid nanocomposites demonstrated the most substantial MCF-7 cell inhibition in the anticancer investigation, with a maximum cell inhibition of 65.45% at 100 g/mL^{-1} [21]. In another study, ciprofloxacin (CIP)-loaded CeO_2-CS hybrid prepared by a green approach was used to test the antibiotic sensitivity of 350 mastitis-positive milk samples [20]. The binary hybrid demonstrated increased antibacterial activity at lower MIC

(8 µg/mL) compared to that of free CIP drug alone. Very recently, CeO_2-CS hybrid was also used to prepare food packaging films which demonstrated excellent strong antimicrobial activity against *E. coli* and *L. monocytogenes.* These reports affirm the application of chitosan-based nanoceria composites to act as effective antibacterial and anticancer agents.

In the present study, a CeO_2/CS/GO ternary nanocomposite was developed using an optimized synthesis route considering the biopotential of the independent nanoparticles. The crystalline nature of CeO_2/CS/GO was confirmed using X-ray diffraction (XRD), and the surface morphology and weight percentage of the elemental compositions were assessed using scanning electron microscopy (SEM) with energy-dispersive X-ray (EDAX). The bonded functional groups were identified using Fourier transform infrared (FT-IR) spectroscopy, and the absorbance of the CeO_2/CS/GO surface was measured using UV-vis-spectroscopy. The developed CeO_2/CS/GO ternary nanocomposite was subjected to anti-cancer, anti-bacterial, antifungal, and hemolysis assay studies to confirm its biological potential (Scheme 1). The best anti-cancer activity was recorded when the MCF-7 cell line was treated with 125 g/mL of the developed CeO_2/CS/GO ternary nanocomposite, and the percentage of live cells was found to be 46.37%. The effective anti-bacterial activity was observed at the maximum concentration (1000 g/mL) of the CeO_2/CS/GO ternary nanocomposite, and the zone of inhibition was found to be 10 mm for *Proteus*, *Salmonella*, *Escherichia coli*, and *Staphylococcus* species. Similarly, the zone of inhibition recorded at 1000 g/mL of the CeO_2/CS/GO ternary nanocomposite with *Aspergillus* species was found to be 4 mm. The absorbance peak was 0.711 for 250 g/disc, which was the effective response recorded in the hemolysis assay.

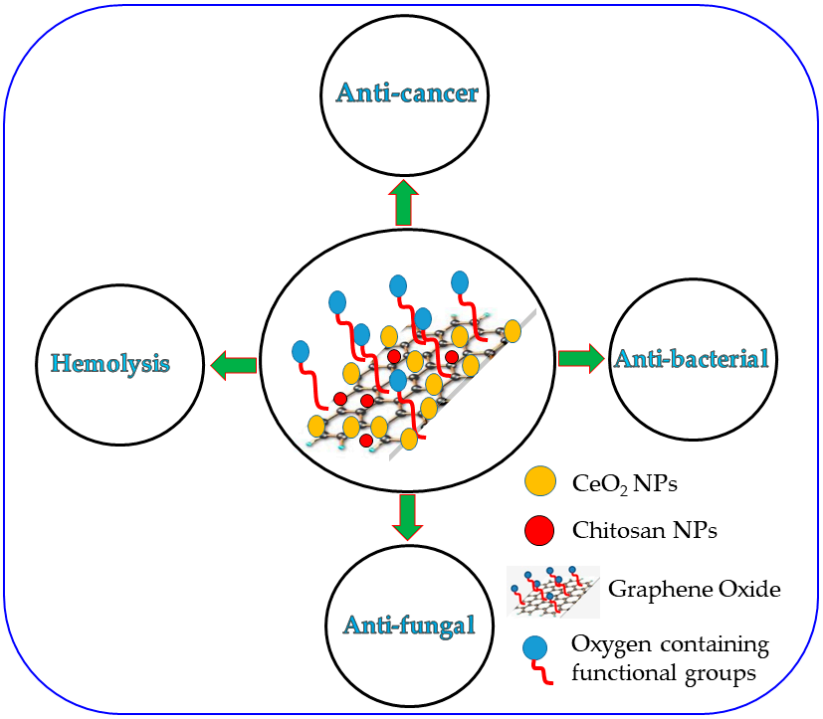

Scheme 1. Schematic representation of CeO_2/CS/GO ternary nanocomposite and its biological activity.

2. Materials and Methods

2.1. Materials

All chemicals and solvents used in this study were of analytical grade. Cerous nitrate hexahydrate ($CeN_3O_9.6H_2O$), graphite powder, sodium nitrate, and sodium hydroxide were purchased from Fisher Science (India). The Alsever solution, which contains water, 2% dextrose, 0.8% sodium citrate, 0.05% citric acid, and 0.42% sodium chloride, as well as isosaline (0.85%, pH 7.2), isosaline (10% *v*/*v*), phosphate buffer (0.15 M, pH 7.3), and hyaline (0.36%) were purchased from Sigma. The XRD pattern of the developed CeO_2/CS/GO

ternary nanocomposite was analyzed using a RIGAKU mini Flux 2C (Japan). The specific cross-functional groups in the CeO_2/CS/GO nanocomposites were determined using FT-IR spectroscopy (JASCO FT-IR-6300, Hachioji, Tokyo, Japan). UV-vis spectroscopy (Model no: DS11, Labman Scientific Instruments, Chennai, Tamil Nadu, India) was used to determine the absorbance of the nanomaterials. The surface of the developed nanostructure was analyzed using a FESEM (SUPRA 55, Carl Zeiss NTS GmBH, Oberkochen, Germany). A Metzer-inverted confocal microscope (METZ-796, Mathura, Uttar Pradesh, India) was used to obtain confocal images of the MCF-7 cell lines.

2.2. Preparation of CeO_2 NPs

CeO_2 was prepared at room temperature using a simple wet chemical procedure. $CeN_3O_9{\cdot}6H_2O$ (0.1 M) was dispersed in 100 mL of distilled water. Subsequently, 50 mL of 0.5 M NaOH solution was added dropwise to 100 mL cerous nitrate hexahydrate and subjected to constant stirring. The resulting mixture was further stirred continuously for 2 h, resulting in a yellow solution that confirmed the formation of CeO_2 NPs. The obtained CeO_2 NPs were cleaned using distilled water and then dried at 150 °C and annealed at 350 °C.

2.3. Preparation of GO NPs

Concentrated H_2SO_4 (46 mL) was mixed with 2 g of graphite powder at 0 °C for 5 min. After the addition of $NaNO_3$ (1 g), the mixture was agitated for 5 min. Subsequently, potassium permanganate (6 g) was gently added to the prepared mixture, which was then agitated for 30 min at 35 °C. H_2O (96 mL) was then added dropwise to the above mixture and the temperature was increased to 98 °C. Upon continuous stirring for 10 min, the initial black color of the mixture changed to reddish-brown, which confirmed the formation of GO NPs.

2.4. Preparation of Chitosan Nanoparticles (CS NPs)

One liter of 1 M HCl was added to demineralize 100 g prawn shells. The reaction was performed for 2–6 h at room temperature and agitated at 250 rpm. The pretreated shells were filtered and washed thoroughly with distilled water of pH 7.0. They were then bleached for 10 min in ethanol and dried in a 70 °C oven for completing the demineralization. The evaporated shells were soaked in distilled water. NaOH (1 M) was added to the shells at a solid/liquid ratio of 1:10. The mixture was reacted with continuous stirring for 3 h at 80 °C, filtered, and rinsed with pure water such that the pH became acidic. The shells were thoroughly cleaned and bleached for 10 min in ethanol, and the resulting chitin was dried at 70 °C, which completed the deproteinization process. Chitin was deacetylated by reacting it with 12.5 M NaOH at a solid/liquid ratio of 1:15 (g/mL). An ultra-freezer was used to chill the reaction mixture and freeze it for 24 h at −83 °C. The reaction was then continued with agitation at 250 rpm for 4 or 6 h, while the mixture's temperature was raised to 115 °C. The chitosan obtained was filtered and washed with pure water to attain a neutral pH at 70 °C.

2.5. Preparation of the CeO_2/CS/GO Ternary Nanocomposite

A total of 1 g of the developed CeO_2 NPs was diluted in 100 mL distilled water and ultrasonicated for 30 min. Subsequently, 1 g GO and 0.5 g CS were individually ultrasonicated for approximately 2 h each. Finally, the two liquids were combined to form a nanocomposite solution. The mixture was blended and agitated for 2 h to produce a homogeneous solution. Finally, the materials were allowed to settle and were washed thrice with distilled water. The CeO_2/CS/GO ternary nanocomposite thus obtained in a (1:0.5:1) ratio was the optimized concentration at which polymer nanocomposites with exceptional structural properties were affirmed using XRD analysis. Here, the concentration of CS was reduced to one-half in comparison with CeO_2 NPs and GO NPs due to its inherent anti-microbial property. The key objective behind this present investigation is to assess

the anti-cancer, anti-bacterial, anti-fungal, and hemolysis biopotentials of the developed CeO_2/CS/GO ternary nanocomposite by fixing equal ratios for CeO_2 and GO NPs and reducing to one-half the ratio of CS which is more dominant in its biological properties.

2.6. In Vitro Anti-Bacterial Assay Using the CeO_2/CS/GO Ternary Nanocomposite

A turbidity standard (0.5 MacFarland tube) was used to standardize 1×10^6 CFU/mL of the inoculums. Wooden applicators with adhering cotton wool swabs were prepared. They were sterilized in tin culture tubes and paper using dry heat or an autoclave. The assay was performed using the gelatin agar disc diffusion technique. Petri plates were set with Muller–Hinton agar (MHA) media, and the bacterial suspensions were added using sterilized cotton swabs dipped in the inoculum. A total of 201 of the standard antibiotic (ampicillin) and sterile samples (in disc form) were added to the MHA plates. The surfaces of the plates were incubated at 37 °C for 24 h. The specimen size was used to determine the effectiveness of the antibacterial agent.

2.7. In Vitro Anti-Fungal Assay Using the CeO_2/CS/GO Ternary Nanocomposite

Standard samples were maintained at 4 °C on a Sabouraud's dextrose agar (SDA) medium. The stock cells were transferred to laboratory tubes containing Sabouraud dextrose broth and incubated for 48 h at ambient temperature to obtain viable cultures for testing. The test was performed using the agar disc diffusion method. The anti-fungal efficacies of the compounds were assessed on an SDA medium using the disc-based dissemination technique. SDA was poured on the Petri plate. After the growth medium had set, the inoculate was spread using a sterilized brush moistened with the fungus solution. The samples were then placed on the surface of the plate. Amphotericin B was used as the control. The prepared plates were incubated at 37 °C for 24 h, after which the width of the resistance area was used to gauge the anti-fungal activity.

2.8. In Vitro MTT Assay Using the CeO_2/CS/GO Ternary Nanocomposite

The MCF-7 cell line was obtained from the King Institute (Guindy, Chennai). The cells were maintained in a minimal essential medium supplemented with 10% fetal bovine serum (FBS; Cistron Laboratories, Coimbatore, Tamil Nadu, India), penicillin (100 U/mL), and streptomycin (100 μg/mL) in a humidified atmosphere of 50 μg/mL CO_2 at 37 °C. Trypsin, methylthiazolyldiphenyl-tetrazolium bromide (MTT), and dimethyl sulfoxide (DMSO) were purchased from Sisco Research Laboratory Chemicals (Mumbai, India). All other chemicals and reagents were obtained from Sigma-Aldrich, Mumbai, India.

After the cells reached confluence, different concentrations of serially diluted samples were added and incubated for 24 h. After incubation, the samples were removed from the wells and washed with phosphate-buffered saline (pH 7.4) or MEM without serum. Then, 100 μL/well (5 mg/mL) of 0.5% MTT was added and incubated for 4 h. Subsequently, 1 mL DMSO was added to each well. The absorbance was measured at 570 nm using a UV-visible spectrophotometer, and DMSO was used as the blank [22]. The concentration required for IC50 was determined graphically. The percentage cell viability was calculated using the following formula:

$$\% \text{ Cell viability} = \text{OD value of treated cells/OD value of control cells} \times 100 \quad (1)$$

2.9. In Vitro Hemolysis Assay Using the CeO_2/CS/GO Ternary Nanocomposite

The hemolysis assay study was performed using the HRBC membrane stabilization technique. The outermost layer of HRBCs is destroyed when exposed to hazardous substances, such as hypotonic fluid, causing hemolysis and breakdown of hemoglobin. As the elements of the HRBC membrane are comparable to those found in lymphocytes, the suppression of the HRBC envelope rupture is used as a proxy for a substance's hemolysis capabilities. Diclofenac sodium was used as the standard. Blood samples were collected from healthy individuals. Equal volumes of sterile Alsever solution, an anticoagulant, and

the collected blood were combined. The packet cells were rinsed with saline (0.85%, pH 7.2) and isosaline (10% v/v) to prepare a solution after centrifuging at 3000 rpm for 5 min. Consequently, the HRBCs were lysed. The experimental mixture contained phosphate buffer (0.15 M, pH 7.4), hyposaline (0.36%), HRBC suspension (0.5 mL), and different quantities of the sample (200, 400, 600, 800, and 1000 g/mL). Double-distilled water (2 mL) was used to prepare a control sample instead of hyposaline. The mixture was incubated at 37 °C for 10 min. Percentage hemolysis was calculated as follows:

$$Percentage\ of\ haemolysis = \frac{100 - OD\ of\ treated\ sample}{OD\ of\ control} \times 100$$

3. Results

3.1. XRD Analysis

Initially, to analyze the biological potential of the cerium oxide/chitosan/graphene oxide (CeO_2/CS/GO), the nanocomposite was prepared in a 1:0.5:1 ratio. In one of the previous reports, 40 mg of chitosan was added to 6 g of CeO_2 NPs, and the resultant CeCh-NPs was subjected to cytotoxicity assessment with the A549 cell line and human foreskin fibroblasts (HFF) cell line. Apoptotic study using flow cytometry, AO/PI stain assay, and antioxidant assay were performed. CeCh-NPs' selective inhibitory impact on A549 cells (IC50: 50.65 g/mL) in comparison with HFF cells (IC50: 131.108) was shown during the evaluation of the cytotoxic effects of CeCh-NPs. This work affirms the cytotoxicity effects of CeCh-NPs with a very minimum concentration of chitosan NP combined with a higher concentration of CeO_2 NPs on cancer cell lines [23]. The purpose of choosing this particular composition was to obtain a highly crystalline composite with superior biological potential. In our previous study, it was revealed that an equivalent composition of a graphene derivative with metal or metal oxide nanoparticles yielded good biological properties of the resulting composite [24]. Thus, the equivalent composition of both CeO_2 and GO was selected. On the other hand, a small amount of chitosan was selected (0.5 g, instead of 1 g in the composite), as the purpose was to test the biological properties of the main contributors, i.e., CeO_2 and GO. Moreover, it was highly likely that a higher amount of chitosan might compromise the crystallinity of the composite [25] while processing the sample. Figure 1 shows the XRD pattern of the CeO_2/CS/GO ternary nanocomposite, which indicates the formation of the nanocomposite. In this composite, the XRD reflections of CeO_2 nanoparticles are indexed and compared with (JCPDS card no: 34-0394), which represents face-centered cubic (*fcc*)-structure CeO_2 nanoparticles. The diffraction peaks appear at ~28.9° (111), ~33.08° (200), 47.47° (220), and 56.36° (311), which suggests the presence of crystalline CeO_2. Notably, some of the XRD peaks are missing, which are possibly suppressed by the high-intensity XRD peak at (111). Apart from these reflections, the chitosan exhibits two peaks: the first peak appears at 2θ = 10.75°, which is only slightly visible and suppressed by another high-intensity peak of chitosan, which is present at 2θ = 20.5°. These peaks correspond to the crystalline structure of chitosan. On the other hand, the characteristic peak of GO also appears and overlaps with the chitosan peak at 2θ = 10.74°, which corresponds to the (001) plane of GO. Furthermore, the XRD analyses of the chitosan and GO and CeO_2 nanoparticles are provided in the supplementary file (Figures S1–S3).

3.2. Surface Morphology

The surface morphology of the CeO_2/CS/GO ternary nanocomposite is shown in Figure 2a,b and its elemental composition is presented in Figure 3 and Table S1, respectively. Figure 3 depicts the elemental compositions of the CeO_2/CS/GO ternary nanocomposites, which included O-36.6, Ce-31.0, S-12.2, and C-8.7, etc. Figure 2a,b affirm the non-agglomerated surface of the developed CeO_2/CS/GO ternary nanocomposite. This surface topography improves the biopotential of the developed CeO_2/CS/GO ternary nanocomposite, and the same is addressed in the below sections.

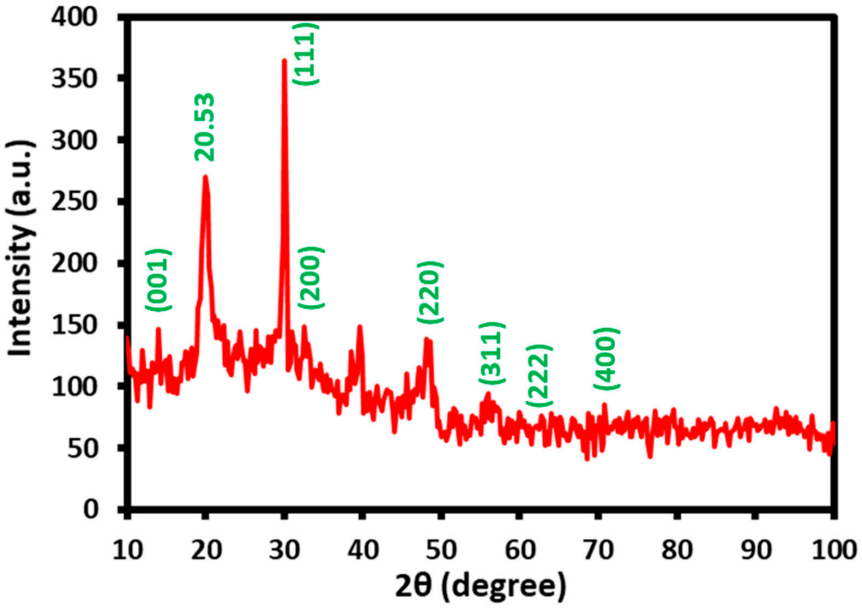

Figure 1. XRD peaks of the CeO_2/CS/GO ternary nanocomposite.

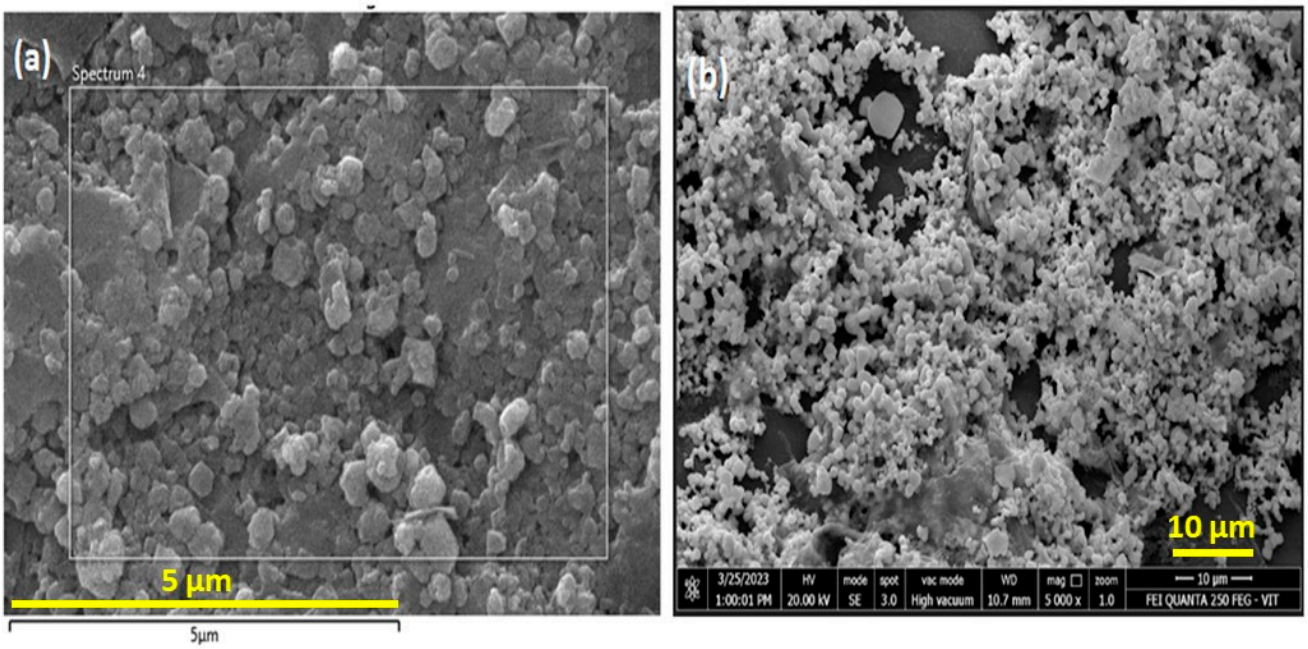

Figure 2. (**a**,**b**) SEM images of the CeO_2/CS/GO ternary nanocomposite.

3.3. FT-IR Analysis

The presence of different functional groups and their bonding in the developed CeO_2/CS/GO ternary nanocomposite were confirmed by recording the FT-IR spectrum of the sample (3500–1000 cm^{-1}), as shown in Figure 4. In this spectrum, the FT-IR peaks of GO can be located at different positions, such as the peaks of hydrogen-bonded O–H (3100–3600 cm^{-1}), C=O (1731 cm^{-1}), C=C (1623 cm^{-1}), and C–O (1222 cm^{-1}, 1053 cm^{-1}). On the other hand, FT-IR peaks of chitosan in the same spectrum can be identified at 3410 cm^{-1} (O–H and N–H), 2925 cm^{-1}, 2854 cm^{-1} (aliphatic C–H), 1655 cm^{-1} (bending vibration N–H), 1420 cm^{-1} (C–N), and 1080 cm^{-1} (C–O). Whereas, FTIR spectra of CeO_2 exhibit different peak positions, such as CeO_2 having a surface hydroxyl group (OH) band located in the region of 3200–3600 cm^{-1}, and carbonate adsorbates on the surface of CeO_2 located by characteristic peaks in the region of 1400–1500 cm^{-1}, corresponding

to the stretching vibrations of carbonate ions. Furthermore, the fingerprint region (below 1500 cm^{-1}) contains smaller peaks and features that are specific to the CeO_2 nanoparticle structure. These can provide additional information about the particle's crystalline phase and purity. The band at 750 cm^{-1} can be attributed to the Ce–O stretching vibrations which ultimately confirm the formation of nanocomposites involving three different components such as GO, chitosan, and CeO_2 nanoparticles. Furthermore, the FT-IR spectra of the chitosan and GO and CeO_2 nanoparticles are provided in the supplementary file (Figures S4–S6).

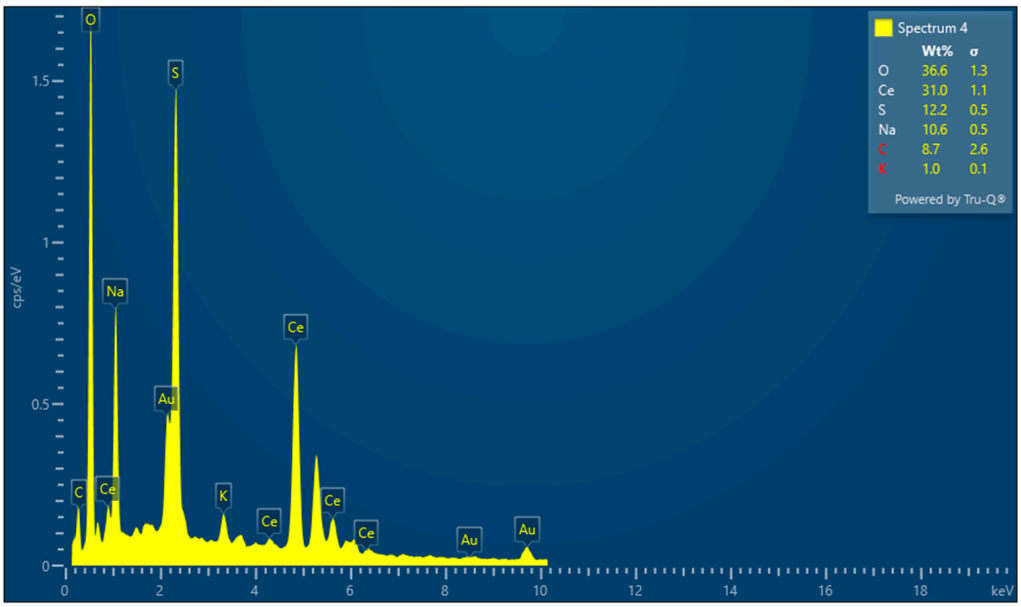

Figure 3. EDAX peaks of the CeO_2/CS/GO ternary nanocomposite.

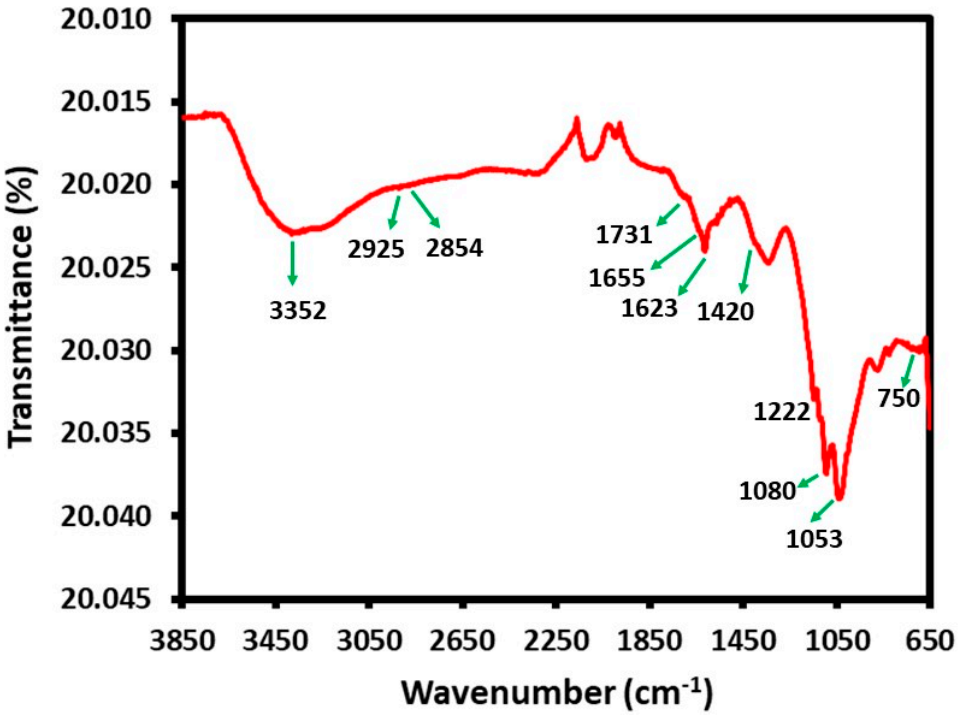

Figure 4. FT-IR analysis of the CeO_2/CS/GO ternary nanocomposite.

3.4. UV-Vis Analysis

The UV spectrum of CS NP, CeO_2 NP, GO, and the CeO_2/CS/GO ternary nanocomposite is shown in Figure 5. This spectrum demonstrates the presence of three different peaks at ~230, ~250, and ~300 nm. Typically, the absorbance peak of CeO_2 NPs can be observed at a wavelength of ~303 nm, which corresponds to the characteristic absorption peak of Ce^{4+} of CeO_2 NPs, which in this case appears at ~300 nm [26]. Similarly, the absorption spectrum of GO consists of two absorption bands which are usually centered at 234 nm is assigned to the π-π* transition of aromatic C–C bonds of graphene lattice, whereas a shoulder band at 298 nm corresponds to the n-π* transition of C=O bond [27]. However, in this study, both these characteristic peaks of GO are overlapped with the absorption peaks of CeO_2 NPs and thus cannot be clearly differentiated. Whereas, the absorption peak at ~250 nm can be attributed to the presence of chitosan, and thus the presence of absorption peaks representing all the components of the composite clearly suggests the formation of CeO_2/CS/GO ternary nanocomposites.

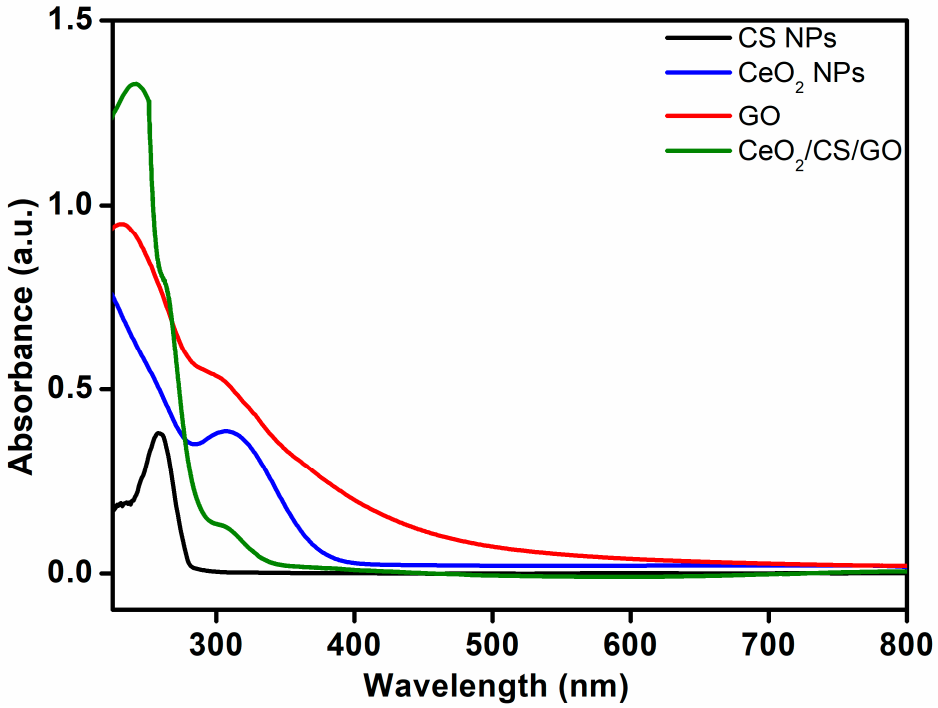

Figure 5. UV analysis of the CeO_2 NPs, CS NPs, GO, and CeO_2/CS/GO ternary nanocomposite.

3.5. Anti-Bacterial Assay

In this study, the CeO_2/CS/GO ternary nanocomposite was prepared in a single-step reaction which was further used to perform biological experiments including anti-bacterial and anti-fungal studies. Notably, such type of ternary composite is rarely used to explore biological potential; however, binary composites involving only chitosan and CeO_2 has been reported in the literature [28]. For instance, Senthilkumar et al. prepared a hybrid involving chitosan and cerium oxide nanoparticles using natural *Sidaacuta* leaf extract [29]. This binary composite at the concentration of 50 µL exhibited considerable morphological changes against *E. coli* and *B. subtilis* organisms due to the direct interaction between chitosan-CeO_2 nanoparticles. Very recently, Appu et al. prepared CS/CeO_2 using aqueous extracts of tea polyphenols. This composite showed an excellent antibacterial and antifungal efficacy against foodborne pathogens including *E. coli*, *S. aureus*, and *B. cinerea* with zones of inhibition of 13.5 ± 0.2 and 11.7 ± 0.2 mm, respectively. However, in the current study, we also included GO which is known to possess significant biological potential, which is reflected in the current ternary composite.

The developed CeO_2/CS/GO ternary nanocomposite was incubated with various bacteria, including *Proteus*, *Salmonella*, *E. coli*, *Staphylococcus*, and *Bacillus* species, using the agar disc diffusion method. The zone of inhibition (ZOI) was 10 mm for all bacteria, excluding *Bacillus* species, at 1000 g/disc of CeO_2/CS/GO nanocomposite. At a minimum concentration of 500 µg/disc of CeO_2/CS/GO nanocomposite, the zone of inhibition (ZOI) was 8 mm for *Salmonella* and *E. coli*, 7 mm for *Staphylococcus* species, and 5 mm for *Proteus* and *Bacillus* species, as shown in Table 1 and Figure 6.

Table 1. Anti-bacterial activity of CeO_2/CS/GO NPs against various bacteria.

S. No.	Microorganisms	*Proteus* Species (ZOI in mm)	*Salmonella* Species (ZOI in mm)	*E. coli* Species (ZOI in mm)	*Staphylococcus* Species (ZOI in mm)	*Bacillus* Species (ZOI in mm)
1	CeO_2/CS/GO ternary nanocomposite (1000 µg/disc)	10	10	10	10	8
2	CeO_2/CS/GO ternary nanocomposite (750 µg/disc)	7	9	9	9	6
3	CeO_2/CS/GO ternary nanocomposite (500 µg/disc)	5	8	8	7	5
A	Ampicillin (antibiotic)	15	20	15	15	13

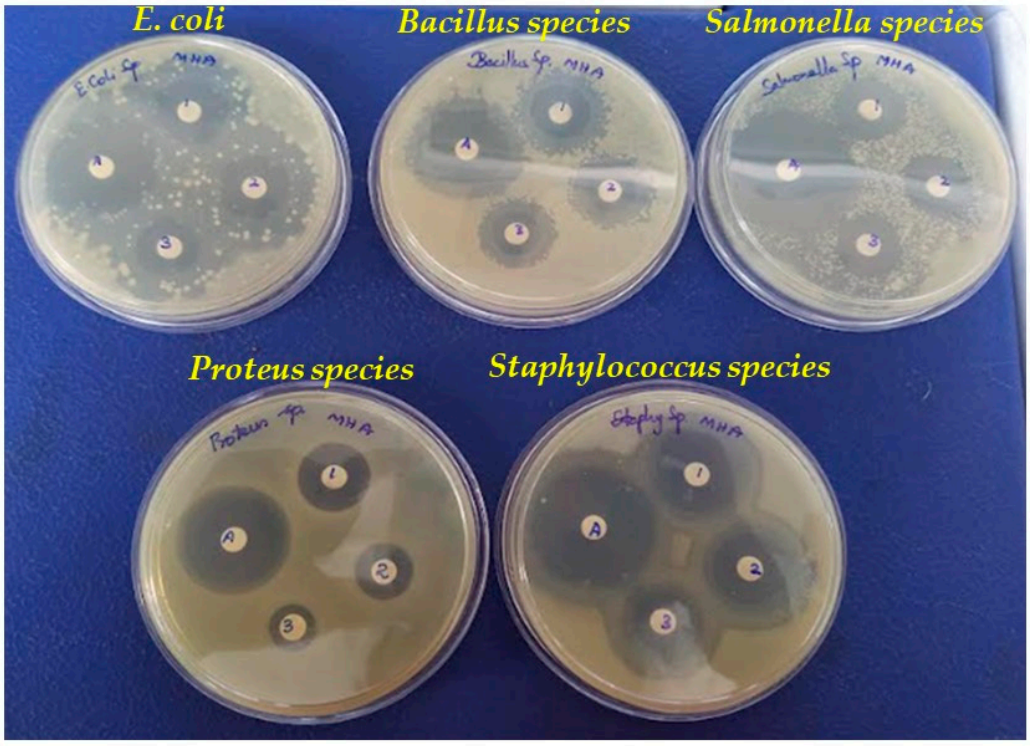

Figure 6. Anti-bacterial activity of CeO_2/CS/GO ternary nanocomposite. *E. coli*, *Bacillus* species, *Salmonella* species, *Proteus* species, and *Staphylococcus* species. ((1) CeO_2/CS/GO ternary nanocomposite (1000 µg/disc), (2) CeO_2/CS/GO ternary nanocomposite (750 µg/disc), (3) CeO_2/CS/GO ternary nanocomposite (500 µg/disc), and (A) Ampicillin (antibiotic)).

In previous reports, lanthanum-doped zinc oxide nanomaterials were incubated with bacteria such as *P. mirabilis*, *S. typhi*, *S. aureus*, and *B. subtilis*. At the maximum concentration of 0.07 µg/mL, the zone of inhibition was 22 mm for *P. mirabilis*, 7 mm for *S. typhi*, and

0 mm for *S. aureus* and *B. subtilis* [30]. Similarly, the anti-bacterial properties of titanium dioxide nanoparticles were analyzed using *S. aureus*, *Serratia marcescens*, and *E. coli*. The zone of inhibition for a maximum concentration of 1000 g/disc was 5 mm for *S. aureus* and *S. marcens*, and 3 mm for *E. coli* [31]. Typically, nanomaterials including nanocomposites exert anti-bacterial mechanisms through various means, including the direct physical interaction of highly sharp edges of a variety of nanomaterials with the corresponding biological entities including membranes of the bacterial cell walls [32]. The second possible mechanism of antibacterial activity of nanomaterials is the generation of reactive oxygen species (ROS), including hydroxyl radicals, superoxide anion, and hydrogen peroxide etc., by the inducing ability of nanoparticles [33,34]. Nanomaterials are known to induce oxidative stress which potentially influences intracellular calcium concentrations, activates transcription factors, and modulates cytokine production via the generation of free radicals [35]. Apart from these, the third possible mechanism is the trapping of bacteria within the aggregated nanomaterials. This mechanism is particularly suitable for layered materials such as graphene derivatives, carbon nitride, etc. [36]. The other mechanisms are the generation of oxidative stress, interruption of the glycolysis process of the bacteria, release of metal ions, contribution to the generation/explosion of nanobubbles, etc. [11,37–39]. In this study, the as-prepared CeO_2/CS/GO ternary nanocomposite may exert antibacterial properties by the combination of both ROS generation and the physical damage to the membranes of the bacterial cell wall. These mechanisms can be attributed to the CeO_2 and graphene oxide in the composite, as CeO_2 is typically known to exert antibacterial activity by ROS generation, while the sharp edges of GO are known to cause physical damage to the bacterial cell wall [40,41]. CeO_2 NPs' antibacterial efficacy in the absence of light depends on concentration. We can observe an expansion of the zone of inhibition as the nanoparticle concentration is raised. The conversion of Ce^{4+} to Ce^{3+} results in oxidative stress on the bacterial membrane as well. CeO_2 NPs are electrostatically drawn to the bacterial cell membrane and adhere there. They experience oxidative stress as a result of the acquisition of electrons through Ce^{4+} to Ce^{3+} conversion. Since gram-positive bacteria have a strong cell wall comprised of peptidoglycan that is difficult to penetrate, gram-negative bacteria are more vulnerable to antibacterial activity than gram-positive bacteria [42].

3.6. Anti-Fungal Assay

The antifungal activity of the developed CeO_2/CS/GO ternary nanocomposite was analyzed against *A. niger* using the agar disc diffusion method, as shown in Figure 7. At the maximum concentration of 1000 µg/disc of CeO_2/CS/GO nanocomposite, the ZOI was recorded to be 4 mm. In contrast, at a minimum concentration of 500 µg/disc of CeO_2/CS/GO nanocomposite, the ZOI was 2 mm (Figure 7). Table 2 presents the ZOI values recorded upon incubating *A. niger* with different nanocomposites. Chitosan may have hindered the integrity of protein biosynthesis and cell surface architecture, which may have had an impact on the growth and development of *Aspergillus ochraceus*. These results have implications for the use of chitosan as an alternative method of fungi pathogen control [43]. In a study, maximum microbial inhibition was demonstrated by CeO_2/GO as a result of the improved photocatalytic activity of cerium oxide and graphene oxide. The transport of photoradicals to the graphene oxide is aided by the light's excitation of cerium nanoparticles attached to graphene sheets. The balance between adsorption and desorption was upset, making it easy for more charged particles to pass across the molecular matrix. Additionally, layer-structured GO aided in the equally distributed nanoparticle distribution, which may have improved photocatalytic activity [44,45].

3.7. Hemolysis Assay

HRBCs were used for assessing the hemolysis activity of the developed CeO_2/GO/CS ternary nanocomposite. Absorbance was recorded upon the interaction of HRBCs with various concentrations of the developed NC. The percentage hemolysis was 0.5 at 1000 µg/disc; at 500 µg/disc, it was 0.696, while it was 0.711 at 250 µg/disc and 125 µg/disc, and 0.622

for the blank (Table S2, Supplementary File). In previous studies on anti-inflammatory responses for copper nanoparticles using HRBCs, percentage hemolysis was recorded to be 0.246 at 200 µg/mL, while it was 0.649 at the lower concentration of 50 µg/mL [50]. Similarly, when silver nanoparticles were analyzed for anti-inflammatory response, the percentage of hemolysis was recorded to be 0.18 for 800 µg/mL and 0.54 for 200 µg/mL [51]. These observations affirm the hemolysis activity of HRBCs. As a part of future work, advanced studies will be carried out to affirm the biopotential of the CeO_2/CS/GO ternary nanocomposite toward the treatment of blood-borne disease.

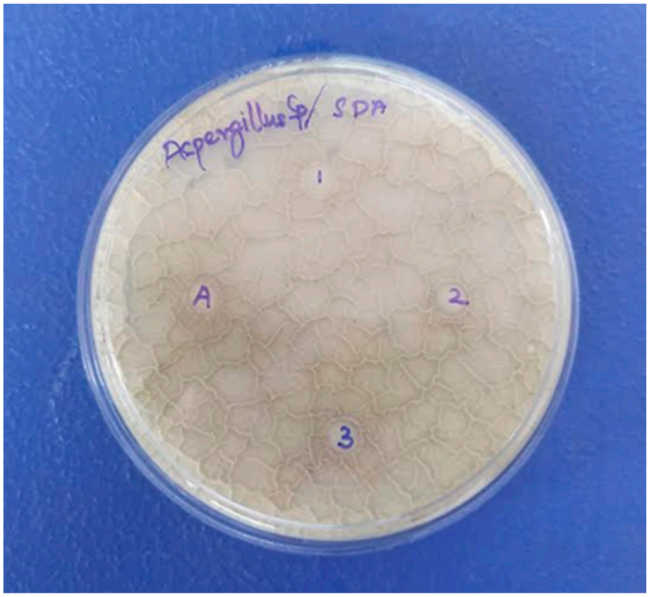

Figure 7. Anti-fungal activity of CeO_2/CS/GO ternary nanocomposite on *Aspergillus niger*.

Table 2. Comparative analysis of different NPs against *Aspergillus niger*.

S. No.	Maximum Concentration of Nanocomposite (1000 µg/disc)	*Aspergillus* Species (ZOI in mm)	References
1	Sodium hydranate titanium dioxide bio-nanocomposite	13.3	[46]
2	Polymer nanocomposite	15	[47]
3	CuO/C nanocomposite	12	[48]
4	Gelatin chitin nanocomposite	10	[49]
5	CeO_2/GO/CS ternary nanocomposite	10	This work

3.8. Anti-Cancer Activity of the CeO_2/CS/GO Ternary Nanocomposite Using MTT Assay

The culture medium containing a minimum of 100,000 MCF-7 cells was incubated with varying concentrations of the CeO_2/CS/GO ternary nanocomposite, and the percentage of live cells was recorded as shown in Table 3. Here, IC50 concentration is defined as the concentration of the CeO_2/CS/GO ternary nanocomposite for which nearly 50% of MCF-7 cancer cells remain dead. Varying concentrations (1000, 500, 250, 125, 62.5, 31.5, 15.6, and 7.8 µg/mL) of the developed CeO_2/CS/GO nanocomposite were used to assess its anti-cancer property against the MCF-7 cell line. The IC50 value was estimated to be 125 µg/mL using Equation (1). The quantitative assessment of the anti-cancer activity of the developed CeO_2/CS/GO nanocomposites at various concentrations is presented in Figure 8. Qualitative assessments were performed from the record of the biochemical interactions of the CeO_2/CS/GO nanocomposite with MCF-7 cells in the culture medium, as presented in Figure 9. As the concentration of the CeO_2/CS/GO nanocomposite increased, the number of cell deaths also increased, which is well presented using various concentrations such as

1000 µg/mL, 250 µg/mL, 125 µg/mL, and 62.5 µg/mL, respectively. Cell death is revealed by the rupture of cells, which leads to a reduction in cell size and a dip in the quantity of cells present in the culture medium, as shown in Figure 9. The %live cells was 18.84 at the maximum concentration of 1000 µg/mL and 85.5 at the minimum concentration of 7.8 µg/mL, respectively. Table 4 presents the mean value plus or minus the standard deviation obtained from the record of the anti-cancer activity of the CeO_2/CS/GO nanocomposite at various concentrations with the MCF-7 cell line three times. For the human foreskin fibroblasts (HFF) and lung cell line (A549), the IC50 of ceria-loaded chitosan nanoparticles (CeCh-NPs) was reported to be 50.65 and 131.108 µg/mL, respectively [28]. According to a previous report, the median chitosan–cerium oxide nanoparticle concentrations against AGS, A459, PC3, and HFF cells were about 156.02, 169.1, 155.8, and 307.5 µg/mL, respectively [52]. In a study, after 48 h of incubation with varying concentrations of CeNPs (10 to 100 µg/mL), it was discovered that the cytotoxic effect of CeNPs on HaCaT (normal cell lines) and MCF-7 (cancer cell lines) suspended in Dulbecco's phosphate buffered saline (DPBS), with a pH of 7.4, is transient, dose-dependent, and depends on the type of cell lines [53]. In another study, a new series of CeO_2NPs having different structures and morphologies such as nickel (Ni)-doped CeO_2, hollow CeO_2 (hCeO_2), and hollow CeO_2/silicon dioxide (SiO_2) (hCeO_2/SiO_2) NPs were synthesized. Additionally, the results showed that hCeO_2/SiO_2NPs had a lower half maximum inhibitory concentration (IC50) (18.625 g/mL) than other synthetic drugs. When compared with tumoral cells (HT-29), all four chemicals had a much lower cytotoxic effect on non-cancerous cells (HFFF2). In comparison with the previous reports, the results obtained from the present investigation demonstrate the excellent anti-cancer activity of the developed CeO_2/CS/GO nanocomposite against MCF-7 cells.

Table 3. Anti-cancer activity of different NPs and hybrids against MCF-7 cell lines.

S. No.	Nanocomposite	% Live Cells at 1000 µg/mL	References
1	CeO_2/GO nanocomposite	19.44	[9]
2	Cu Fe_2O_4/HYPS nanocomposite	21.23	[54]
3	GO/CS nanocomposite	23.8	[55]
4	Mn/CeO_2 nanocomposite	22.58	[56]
5	CeO_2/GO/CS ternary nanocomposite	18.84	This work

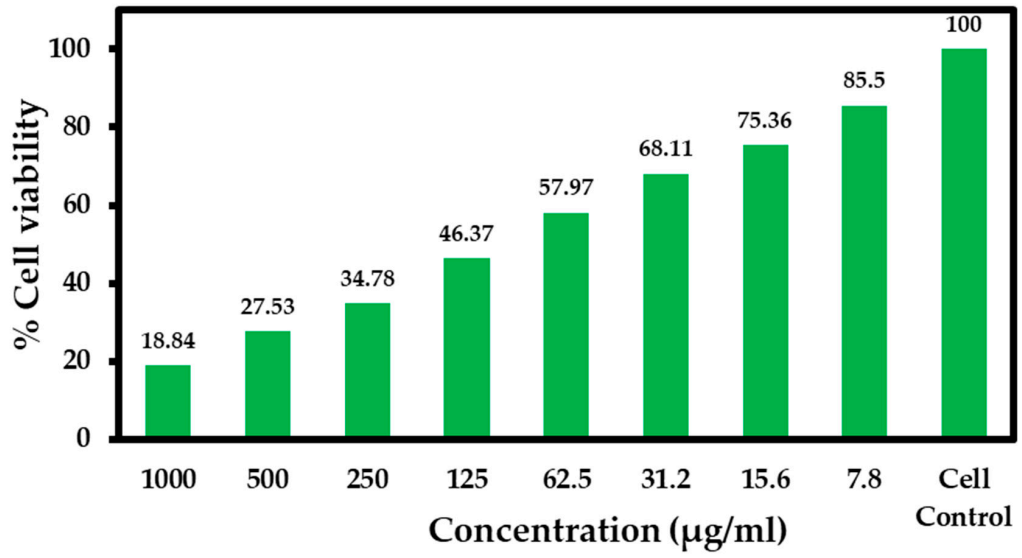

Figure 8. Percentage cell viability of the MCF-7 cell line after treatment with the CeO_2/CS/GO nanocomposite using MTT assay.

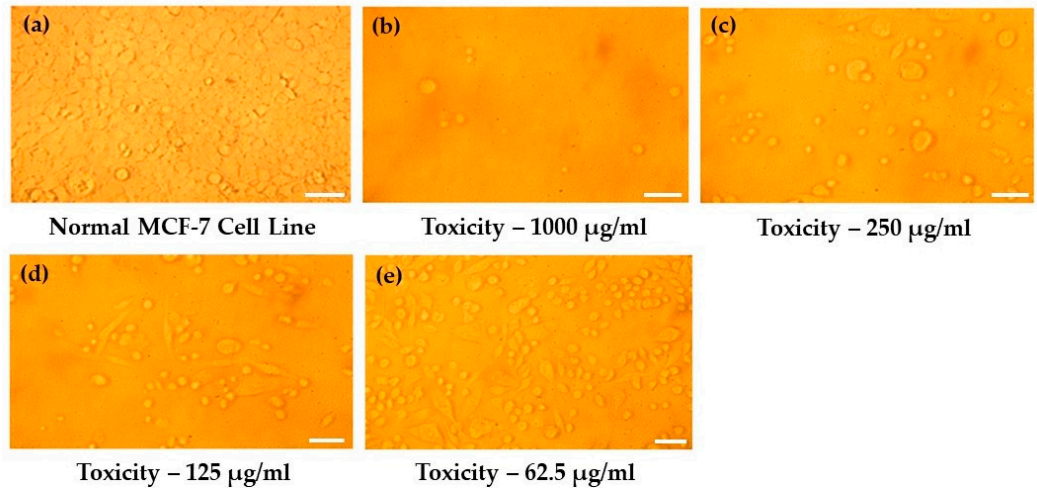

Figure 9. Microscopic images containing untreated MCF-7 cells and the treated behavior of the CeO_2/CS/GO with MCF-7 cell line. All the images were acquired with an objective lens of 20× magnification. Scale bars show 20 µm (**a**–**c**) and 10 µm (**d**,**e**).

Table 4. Anticancer activity of CeO_2/CS/GO ternary nanocomposite on MCF-7 cell line using MTT assay.

S. No	Concentration (µg/mL)	Cell Viability (% Live Cells)
1.	1000	18.84 ± 0.48
2.	500	27.53 ± 0.31
3.	250	34.78 ± 0.35
4.	125	46.37 ± 0.12
5.	62.5	57.97 ± 0.26
6.	31.2	68.11 ± 0.27
7.	15.6	75.36 ± 1.19
8.	7.8	85.50 ± 0.34
9.	Cell control	100 ± 0.45

Mean value ± Standard Deviation (Three replicates).

4. Conclusions

A CeO_2/CS/GO ternary nanocomposite was prepared using a cost-effective wet chemical procedure. The physicochemical properties of the developed CeO_2/CS/GO nanocomposite were confirmed using XRD spectroscopy, SEM with EDAX, FT-IR spectroscopy, and UV-vis spectroscopy. The biological potential of the developed CeO_2/CS/GO nanocomposite was confirmed by performing in vitro anti-bacterial, anti-fungal, anti-cancer, and hemolysis studies. Based on our observations, we affirm inherent anti-cancer activity with the MCF-7 cell line; anti-fungal activity with Aspergillus niger; anti-bacterial activity with *E. coli*, *Bacillus* species, *Salmonella* species, Proteus species, and *staphylococcus* species; and hemolysis response with HRBCs. As a part of future work, quantitative and qualitative studies can be conducted with the developed CeO_2/CS/GO nanocomposite through its interaction with other types of cancer cell lines, bacterial cell lines, and fungal cell lines. Furthermore, an anti-cancer drug can be introduced in the developed CeO_2/CS/GO nanocomposite, and its efficacy as a drug delivery platform can also be assessed.

Supplementary Materials: The following are available online at https://www.mdpi.com/article/10.3390/cryst13091393/s1. Figure S1: XRD analysis of Chitosan; Figure S2: XRD analysis of GO; Figure S3: XRD analysis of CeO_2; Figure S4: FT-IR analysis of Chitosan; Figure S5: FT-IR analysis of GO; Figure S6: FT-IR analysis of CeO_2; Figure S7: Hemolysis assay using the CeO_2/CS/GO ternary nanocomposite; Table S1: Elemental composition of the CeO_2/CS/GO ternary nanocomposite; Table S2: Hemolysis assay response upon interaction of CeO_2/CS/GO ternary nanocomposite with HRBCs.

Author Contributions: Conceptualization, J.S.; methodology, J.S. and S.P.; validation, J.S. and S.P.; formal analysis, M.R.S., M.K. (Mujeeb Khan) and B.S.; investigation, J.S. and S.P.; resources, J.S. and M.R.S.; data curation, S.P., M.R.S., M.K. (Merajuddin Khan) and B.S.; writing—original draft preparation, J.S., S.P. and M.R.S.; writing—review and editing, J.S., M.R.S., M.K. (Merajuddin Khan) and M.K. (Mujeeb Khan); supervision, J.S.; project administration, J.S.; funding acquisition, M.R.S. All authors have read and agreed to the published version of the manuscript.

Funding: This research was funded by Researchers Supporting Project number (RSPD2023R665), King Saud University, Riyadh, Saudi Arabia.

Institutional Review Board Statement: Not applicable.

Informed Consent Statement: Not applicable.

Data Availability Statement: Data contained within the article.

Acknowledgments: The authors acknowledge the funding from Researchers Supporting Project number (RSPD2023R665), King Saud University, Riyadh, Saudi Arabia.

Conflicts of Interest: The authors declare no conflict of interest.

References

1. Saeedi, M.; Vahidi, O.; Moghbeli, M.; Ahmadi, S.; Asadnia, M.; Akhavan, O.; Seidi, F.; Rabiee, M.; Saeb, M.R.; Webster, T.J. Customizing nano-chitosan for sustainable drug delivery. *J. Control Release* **2022**, *350*, 175–192. [CrossRef]
2. Emilian Leucuta, S. Nanotechnology for delivery of drugs and biomedical applications. *Curr. Clin. Pharmacol.* **2010**, *5*, 257–280. [CrossRef] [PubMed]
3. Dai, X.; Cheng, H.; Bai, Z.; Li, J. Breast cancer cell line classification and its relevance with breast tumor subtyping. *J. Cancer* **2017**, *8*, 3131. [CrossRef] [PubMed]
4. Maleki, P.; Nemati, F.; Gholoobi, A.; Hashemzadeh, A.; Sabouri, Z.; Darroudi, M. Green facile synthesis of silver-doped cerium oxide nanoparticles and investigation of their cytotoxicity and antibacterial activity. *Inorg. Chem. Commun.* **2021**, *131*, 108762. [CrossRef]
5. Dhall, A.; Self, W. Cerium oxide nanoparticles: A brief review of their synthesis methods and biomedical applications. *Antioxidants* **2018**, *7*, 97. [CrossRef]
6. Tsunekawa, S.; Sivamohan, R.; Ohsuna, T.; Takahashi, H.; Tohji, K. Ultraviolet absorption spectra of CeO_2 nano-particles. In *Materials Science Forum*; Trans Tech Publications Ltd.: Wollerau, Switzerland, 1999; pp. 439–445.
7. Saranya, J.; Sreeja, B.; Padmalaya, G.; Radha, S.; Manikandan, T. Ultrasonic assisted cerium oxide/graphene oxide hybrid: Preparation, anti-proliferative, apoptotic induction and G2/M cell cycle arrest in HeLa cell lines. *J. Inorg. Organomet. Polym. Mater.* **2020**, *30*, 2666–2676. [CrossRef]
8. Çiplak, Z.; Yildiz, N.; Çalimli, A. Investigation of graphene/Ag nanocomposites synthesis parameters for two different synthesis methods. *Fuller. Nanotub. Carbon Nanostructures* **2015**, *23*, 361–370. [CrossRef]
9. Saranya, J.; Saminathan, P.; Ankireddy, S.R.; Shaik, M.R.; Khan, M.; Khan, M.; Shaik, B. Cerium Oxide/Graphene Oxide Hybrid: Synthesis, Characterization, and Evaluation of Anticancer Activity in a Breast Cancer Cell Line (MCF-7). *Biomedicines* **2023**, *11*, 531. [CrossRef]
10. Pang, L.; Dai, C.; Bi, L.; Guo, Z.; Fan, J. Biosafety and antibacterial ability of graphene and graphene oxide in vitro and in vivo. *Nanoscale Res. Lett.* **2017**, *12*, 564. [CrossRef]
11. Liu, S.; Zeng, T.H.; Hofmann, M.; Burcombe, E.; Wei, J.; Jiang, R.; Kong, J.; Chen, Y. Antibacterial activity of graphite, graphite oxide, graphene oxide, and reduced graphene oxide: Membrane and oxidative stress. *ACS Nano* **2011**, *5*, 6971–6980. [CrossRef]
12. Kayani, F.B.; Rafique, S.; Akram, R.; Hussain, M.; Raja, K.; Khan, J.S. Fabrication of novel chitosan@Ag/CeO_2 hybrid nanocomposites for the study of antibacterial activity. *Phys. E Low-Dimens. Syst. Nanostructures* **2023**, *149*, 115683. [CrossRef]
13. Panda, P.K.; Dash, P.; Yang, J.-M.; Chang, Y.-H. Development of chitosan, graphene oxide, and cerium oxide composite blended films: Structural, physical, and functional properties. *Cellulose* **2022**, *29*, 2399–2411. [CrossRef]
14. Mali, S.; Nune, K.; Misra, R. Biomimetic nanostructured hydroxyapatite coatings on metallic implant materials. *Mater. Technol.* **2016**, *31*, 782–790. [CrossRef]
15. Pimenta, J.A.; Zaparolli, D.; Pécora, J.D.; Cruz-Filho, A.M. Chitosan: Effect of a new chelating agent on the microhardness of root dentin. *Braz. Dent. J.* **2012**, *23*, 212–217. [CrossRef] [PubMed]
16. Alimirzaei, F.; Vasheghani-Farahani, E.; Ghiaseddin, A.; Soleimani, M. pH-Sensitive Chitosan Hydrogel with Instant Gelation for Myocardial Regeneration. *J. Tissue Sci. Eng.* **2017**, *8*, 3.
17. de Sousa Victor, R.; Marcelo da Cunha Santos, A.; Viana de Sousa, B.; de Araújo Neves, G.; Navarro de Lima Santana, L.; Rodrigues Menezes, R. A review on Chitosan's uses as biomaterial: Tissue engineering, drug delivery systems and cancer treatment. *Materials* **2020**, *13*, 4995.
18. Anjum, S.; Arora, A.; Alam, M.; Gupta, B. Development of antimicrobial and scar preventive chitosan hydrogel wound dressings. *Int. J. Pharm.* **2016**, *508*, 92–101. [CrossRef]

19. Zaboon, M.H.; Saleh, A.A.; Al-Lami, H.S. Synthesis, characterization and cytotoxicity investigation of chitosan-amino acid derivatives nanoparticles in human breast cancer cell lines. *J. Mex. Chem. Soc.* **2021**, *65*, 178–188. [CrossRef]
20. Appu, M.; Wu, H.; Chen, H.; Huang, J. Tea polyphenols mediated biogenic synthesis of chitosan-coated cerium oxide (CS/CeO_2) nanocomposites and their potent antimicrobial capabilities. *Environ. Sci. Pollut. Res.* **2023**, *30*, 42575–42586. [CrossRef]
21. Kasinathan, K.; Murugesan, B.; Pandian, N.; Mahalingam, S.; Selvaraj, B.; Marimuthu, K. Synthesis of biogenic chitosan-functionalized 2D layered MoS2 hybrid nanocomposite and its performance in pharmaceutical applications: In-Vitro antibacterial and anticancer activity. *Int. J. Biol. Macromol.* **2020**, *149*, 1019–1033. [CrossRef]
22. Mosmann, T. Rapid colorimetric assay for cellular growth and survival: Application to proliferation and cytotoxicity assays. *J. Immunol. Methods* **1983**, *65*, 55–63. [CrossRef] [PubMed]
23. Abbasi, N.; Homayouni Tabrizi, M.; Ardalan, T.; Roumi, S. Cerium oxide nanoparticles-loaded on chitosan for the investigation of anticancer properties. *Mater. Technol.* **2022**, *37*, 1439–1449. [CrossRef]
24. Adil, S.F.; Shaik, M.R.; Nasr, F.A.; Alqahtani, A.S.; Ahmed, M.Z.; Qamar, W.; Kuniyil, M.; Almutairi, A.; Alwarthan, A.; Siddiqui, M.R.H. Enhanced apoptosis by functionalized highly reduced graphene oxide and gold nanocomposites in MCF-7 breast cancer cells. *ACS Omega* **2021**, *6*, 15147–15155. [CrossRef] [PubMed]
25. Ioelovich, M. Crystallinity and hydrophility of chitin and chitosan. *J. Chem.* **2014**, *3*, 7–14.
26. Nurhasanah, I.; Safitri, W.; Arifin, Z.; Subagio, A.; Windarti, T. *Antioxidant Activity and Dose Enhancement Factor of CeO_2 Nanoparticles Synthesized by Precipitation Method*; IOP Conference Series: Materials Science and Engineering; IOP Publishing Ltd.: Bristol, UK, 2018; p. 012031.
27. Wang, S.; Zhang, Y.; Ma, H.-L.; Zhang, Q.; Xu, W.; Peng, J.; Li, J.; Yu, Z.-Z.; Zhai, M. Ionic-liquid-assisted facile synthesis of silver nanoparticle-reduced graphene oxide hybrids by gamma irradiation. *Carbon* **2013**, *55*, 245–252. [CrossRef]
28. Sanmugam, A.; Abbishek, S.; Kumar, S.L.; Sairam, A.B.; Palem, V.V.; Kumar, R.S.; Almansour, A.I.; Arumugam, N.; Vikraman, D. Synthesis of chitosan based reduced graphene oxide-CeO_2 nanocomposites for drug delivery and antibacterial applications. *J. Mech. Behav. Biomed. Mater.* **2023**, *145*, 106033. [CrossRef]
29. Senthilkumar, R.; Bhuvaneshwari, V.; Ranjithkumar, R.; Sathiyavimal, S.; Malayaman, V.; Chandarshekar, B. Synthesis, characterization and antibacterial activity of hybrid chitosan-cerium oxide nanoparticles: As a bionanomaterials. *Int. J. Biol. Macromol.* **2017**, *104*, 1746–1752. [CrossRef]
30. Manikandan, A.; Manikandan, E.; Meenatchi, B.; Vadivel, S.; Jaganathan, S.; Ladchumananandasivam, R.; Henini, M.; Maaza, M.; Aanand, J.S. Rare earth element (REE) lanthanum doped zinc oxide (La: ZnO) nanomaterials: Synthesis structural optical and antibacterial studies. *J. Alloys Compd.* **2017**, *723*, 1155–1161. [CrossRef]
31. Gudata, L.; Saka, A.; Tesfaye, J.L.; Shanmugam, R.; Dwarampudi, L.P.; Nagaprasad, N.; Stalin, B.; Krishnaraj, R. Investigation of TiO2 nanoparticles using leaf extracts of Lippia adoensis (Kusaayee) for antibacterial activity. *J. Nanomater.* **2022**, *2022*, 3881763. [CrossRef]
32. Akhavan, O.; Ghaderi, E. Toxicity of graphene and graphene oxide nanowalls against bacteria. *ACS Nano* **2010**, *4*, 5731–5736. [CrossRef]
33. Dutta, T.; Sarkar, R.; Pakhira, B.; Ghosh, S.; Sarkar, R.; Barui, A.; Sarkar, S. ROS generation by reduced graphene oxide (rGO) induced by visible light showing antibacterial activity: Comparison with graphene oxide (GO). *RSC Adv.* **2015**, *5*, 80192–80195. [CrossRef]
34. Lakshmi Prasanna, V.; Vijayaraghavan, R. Insight into the mechanism of antibacterial activity of ZnO: Surface defects mediated reactive oxygen species even in the dark. *Langmuir* **2015**, *31*, 9155–9162. [CrossRef]
35. Canaparo, R.; Foglietta, F.; Limongi, T.; Serpe, L. Biomedical applications of reactive oxygen species generation by metal nanoparticles. *Materials* **2020**, *14*, 53. [CrossRef] [PubMed]
36. Akhavan, O.; Ghaderi, E.; Esfandiar, A. Wrapping bacteria by graphene nanosheets for isolation from environment, reactivation by sonication, and inactivation by near-infrared irradiation. *J. Phys. Chem. B* **2011**, *115*, 6279–6288. [CrossRef] [PubMed]
37. Akhavan, O.; Ghaderi, E. Escherichia coli bacteria reduce graphene oxide to bactericidal graphene in a self-limiting manner. *Carbon* **2012**, *50*, 1853–1860. [CrossRef]
38. Wang, Y.-W.; Cao, A.; Jiang, Y.; Zhang, X.; Liu, J.-H.; Liu, Y.; Wang, H. Superior antibacterial activity of zinc oxide/graphene oxide composites originating from high zinc concentration localized around bacteria. *ACS Appl. Mater. Interfaces* **2014**, *6*, 2791–2798. [CrossRef] [PubMed]
39. Jannesari, M.; Akhavan, O.; Hosseini, H.R.M.; Bakhshi, B. Oxygen-rich graphene/ZnO_2-Ag nanoframeworks with pH-switchable catalase/peroxidase activity as O2 nanobubble-self generator for bacterial inactivation. *J. Colloid Interface Sci.* **2023**, *637*, 237–250. [CrossRef]
40. Zhang, M.; Zhang, C.; Zhai, X.; Luo, F.; Du, Y.; Yan, C. Antibacterial mechanism and activity of cerium oxide nanoparticles. *Sci. China Mater.* **2019**, *62*, 1727–1739. [CrossRef]
41. Nanda, S.S.; Yi, D.K.; Kim, K. Study of antibacterial mechanism of graphene oxide using Raman spectroscopy. *Sci. Rep.* **2016**, *6*, 28443. [CrossRef]
42. Sawai, J. Quantitative evaluation of antibacterial activities of metallic oxide powders (ZnO, MgO and CaO) by conductimetric assay. *J. Microbiol. Methods* **2003**, *54*, 177–182. [CrossRef]
43. Meng, D.; Garba, B.; Ren, Y.; Yao, M.; Xia, X.; Li, M.; Wang, Y. Antifungal activity of chitosan against Aspergillus ochraceus and its possible mechanisms of action. *Int. J. Biol. Macromol.* **2020**, *158*, 1063–1070. [CrossRef] [PubMed]

44. Egorova, M.N.; Tarasova, L.A.; Vasilieva, F.D.; Akhremenko, Y.A.; Smagulova, S.A. Antimicrobial activity of graphene oxide sheets. In Proceedings of the AIP Conference Proceedings, Yakutsk, Russia, 18–23 June 2018; AIP Publishing: Long Island, NY, USA.
45. Cao, M.; Wang, P.; Ao, Y.; Wang, C.; Hou, J.; Qian, J. Visible light activated photocatalytic degradation of tetracycline by a magnetically separable composite photocatalyst: Graphene oxide/magnetite/cerium-doped titania. *J. Colloid Interface Sci.* **2016**, *467*, 129–139. [CrossRef] [PubMed]
46. Safaei, M.; Taran, M. Fabrication, characterization, and antifungal activity of sodium hyaluronate-TiO_2 bionanocomposite against Aspergillus niger. *Mater. Lett.* **2017**, *207*, 113–116. [CrossRef]
47. Hasanin, M.; Hashem, A.H.; Lashin, I.; Hassan, S.A. In vitro improvement and rooting of banana plantlets using antifungal nanocomposite based on myco-synthesized copper oxide nanoparticles and starch. *Biomass Convers. Biorefin.* **2021**, *13*, 8865–8875. [CrossRef]
48. Roopan, S.M.; Priya, D.D.; Shanavas, S.; Acevedo, R.; Al-Dhabi, N.A.; Arasu, M.V. CuO/C nanocomposite: Synthesis and optimization using sucrose as carbon source and its antifungal activity. *Mater. Sci. Eng. C* **2019**, *101*, 404–414. [CrossRef]
49. Sahraee, S.; Milani, J.M.; Ghanbarzadeh, B.; Hamishehkar, H. Physicochemical and antifungal properties of bio-nanocomposite film based on gelatin-chitin nanoparticles. *Int. J. Biol. Macromol.* **2017**, *97*, 373–381. [CrossRef]
50. Anitha, P.; Sakthivel, P. Microwave Assisted Synthesis and Characterization of Silver Nanoparticles Using Citrullus Lanatus Leaf Extract and Its Anti-Inflammatory Activity Against Human Blood Cells. *Int. J. Adv. Eng. Nano Technol.* **2016**, *3*, 3.
51. Rajeshkumar, S.; Menon, S.; Ponnanikajamideen, M.; Ali, D.; Arunachalam, K. Anti-inflammatory and antimicrobial potential of Cissus quadrangularis-assisted copper oxide nanoparticles. *J. Nanomater.* **2021**, *2021*, 5742981. [CrossRef]
52. Kermani, G.; Karimi, E.; Tabrizi, M.H. Hybrid nanoarchitectonics of chitosan-cerium oxide nanoparticles for anticancer potentials. *J. Inorg. Organomet. Polym. Mater.* **2022**, *32*, 2591–2599. [CrossRef]
53. Yang, K.; Wan, J.; Zhang, S.; Zhang, Y.; Lee, S.-T.; Liu, Z. In vivo pharmacokinetics, long-term biodistribution, and toxicology of PEGylated graphene in mice. *ACS Nano* **2011**, *5*, 516–522. [CrossRef]
54. Jermy, R.; Ravinayagam, V.; Alamoudi, W.; Almohazey, D.; Elanthikkal, S.; Dafalla, H.; Rehman, S.; Chandrasekar, G.; Baykal, A. Tuning pH sensitive chitosan and cisplatin over spinel ferrite/silica nanocomposite for anticancer activity in MCF-7 cell line. *J. Drug Deliv. Sci. Technol.* **2020**, *57*, 101711. [CrossRef]
55. Doghish, A.S.; El-Sayyad, G.S.; Sallam, A.-A.M.; Khalil, W.F.; El Rouby, W.M. Graphene oxide and its nanocomposites with EDTA or chitosan induce apoptosis in MCF-7 human breast cancer. *RSC Adv.* **2021**, *11*, 29052–29064. [CrossRef] [PubMed]
56. Atif, M.; Iqbal, S.; Fakhar-E-Alam, M.; Ismail, M.; Mansoor, Q.; Mughal, L.; Aziz, M.H.; Hanif, A.; Farooq, W. Manganese-doped cerium oxide nanocomposite induced photodynamic therapy in MCF-7 cancer cells and antibacterial activity. *Biomed Res. Int.* **2019**, *2019*, 7156828. [CrossRef] [PubMed]